*Advanced Optical Materials*

ADVANCED OPTICAL MATERIALS
www.advopticalmat.de

RESEARCH ARTICLE OPEN ACCESS

# Aerosol Jet Printed Polymer-Free High Aspect Ratio Quantum Dot Films for Enhanced Color Conversion

Sukyung Choi[1] | Anna Meredith[2] | Hyunsu Cho[1] | Zahra Bahrami[3] | Kevin Schnittker[2] | Joseph Andrews[2,3]

[1]Reality Display Research Section, Electronic and Telecommunications Research Institute (ETRI), Daejeon, Republic of Korea | [2]Department of Mechanical Engineering, Mechanical Engineering Building, University of Wisconsin–Madison, Madison, Wisconsin, USA | [3]Department of Electrical Engineering, Engineering Hall, University of Wisconsin–Madison, Madison, Wisconsin, USA

**Correspondence:** Joseph Andrews (joseph.andrews@wisc.edu)

**Received:** 3 February 2026 | **Revised:** 19 May 2026 | **Accepted:** 22 May 2026

**Keywords:** color conversion | printed electronics | printed optical materials | quantum Dots

## ABSTRACT

Quantum dot (QD) color conversion layers (CCLs) are a promising route toward wide color gamut, simplified display architectures. However, simultaneously achieving high optical quality, fine patterning resolution, and scalable processing remains challenging. Here, we report a polymer-free aerosol jet printing approach for fabricating high-aspect-ratio QD CCLs with precisely controlled morphology and optical performance. By tuning the aerosol focus ratio to induce in-flight droplet drying, we achieve pinned contact-line deposition that enables multilayer QD films with thicknesses up to approximately 10 μm while maintaining lateral feature widths of approximately 50 μm. These polymer-free QD films exhibit strong blue-light absorption and efficient wavelength down-conversion, yielding blue light leakage below 0.25% and conversion efficiencies approaching 18% without the use of external color filters. The printed QD layers are integrated directly onto blue OLED unit devices and a 0.7-inch OLED-on-silicon (OLEDoS) microdisplay, demonstrating high-purity red emission with no degradation of device electrical performance. This work establishes aerosol jet printing as a powerful materials processing strategy for scalable, high-resolution QD color conversion in next-generation microdisplay and near-eye display technologies.

## 1 | Introduction

The introduction of quantum dot color conversion layers (QD CCLs) into organic light-emitting diode (OLED) and micro light-emitting diode (μLED) displays has numerous advantages in terms of enhancing display quality and reducing manufacturing complexity [1–3]. The color gamut of the display can be enhanced due to the high tunability and narrow emission bandwidth of the color converting quantum dots (QDs) [4]. Additionally, the number of steps required to fabricate a red-green-blue (RGB) display pixel can be reduced as each RGB pixel can consist of a single-color emitter coupled with a QD CCL to obtain full RGB emission [5]. The most common architecture employed in such a QD color conversion-enabled display is to use blue OLEDs/μLEDs for each sub-pixel with an associated red and green color-converting quantum dot thin films on the red and green sub-pixels, respectively [6]. Such displays have been demonstrated in recent literature works and commercial products, capturing the quality, complexity, and energy advantages discussed above.

While the advantages are evident, the process of patterning QDs within this display architecture is challenging [7]. The most prominent methods for QD patterning include photolithography [8] and inkjet printing [3, 5, 9, 10]. Photolithography has

Sukyung Choi and Anna Meredith contributed equally to this work.

advantages in terms of resolution, even demonstrating the ability to pattern features down to 30 nm [11, 12]; however, the subsequent patterning of multiple layers causes significant challenges. Primarily, this is due to the lack of compatibility between quantum dots and photoresist chemicals. Patterning for RGB compatibility requires multiple deposition steps, in which one QD CCL is deposited first, and therefore, remains on the substrate during the subsequent patterning of an additional quantum dot layer [13]. Another challenge is the photosensitivity of the QDs and associated ligands to ultra-violet light. The incompatibility with photoresists and the photosensitivity of QD ligands have both been demonstrated to lead to decreased performance, or even the dissolution, of the existing QD layer.

Inkjet printing presents a viable alternative to photolithography because the additive nature precludes the need for the use of incompatible photoresists [3, 5, 14]. Due to the stability of QD in solution, inks can be synthesized and subsequently printed directly at specified locations, eliminating the need for subtractive photolithography steps [15]. The primary challenges from inkjet printing include the surface interaction with the substrate and the inability to print fine features due to the surface-limited deposition spot size, which is on the order of 30 μm for most commercially available and custom inkjet printer systems [16]. Additionally, as the QD solution is deposited in the liquid state, there is a tendency to spread, and therefore a pre-patterning step with a polymeric matrix is required to reduce sub-pixel crosstalk [17]. One of the key challenges with inkjet printing in general, and one that significantly impacts QD CCLs is the "coffee-ring effect" [18]. This effect causes the individual QDs to follow the outer concentric flow-field induced by the droplet drying process, resulting in denser films at the outer edges of the surface. This has been sufficiently reduced in recent works by modifying the ink through the use of co-solvents or through pre-patterning the surface with a thick black matrix.

Both methods have one challenge in common, which is the requirement of higher viscosity solutions. To obtain high viscosity QD solutions and to prevent QD agglomeration, it is common to use polymeric additives. These polymeric additives remain in the resultant thin-film and therefore significantly affect the blue-light leakage properties of the QD films [19]. Due to this, many works also incorporate an additional color filter to avoid the leakage of the underlying light emitter.

Other techniques that have been demonstrated in literature include screen printing [20, 21], electrohydrodynamic printing [22–24], aerosol spray printing [25], and micro transfer printing [26]. All of these techniques have benefits, but ultimately present tradeoffs including resolution, color conversion efficiency, blue-light blocking, and processing speed.

Aerosol jet printing offers an attractive method to spatially pattern nanomaterial thin films at higher resolutions when compared to inkjet printing. The process relies on first aerosolizing the ink through either an ultrasonic or pneumatic method. In this work, we utilize ultrasonication due to its compatibility with small ink volumes and more stable operation. In ultrasonic aerosolization, surface capillary waves are created through an ultrasonic transducer, causing droplet pinch off [27]. The droplet size distribution is on the order of 1–5 μm and is largely determined by the surface tension of the ink [28]. The droplets are then transported using an inert carrier gas to a deposition head, where the aerosol stream is aerodynamically focused using an additional sheath gas. The operating principles are displayed in the schematic presented in Figure 1.

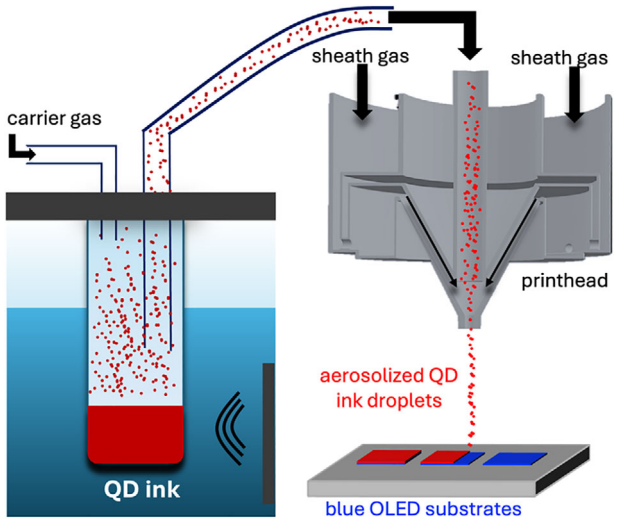


**FIGURE 1** | Schematic of the aerosol jet printing process depicting the ultrasonic droplet generation, droplet transport, aerodynamic focusing, and substrate impingement.

This method has numerous differentiating advantages when compared to inkjet printing, especially for printing nanomaterials such as QDs. For one, the process is compatible with viscosities as low as 1 cP, enabling the printing of QD inks formed without polymeric additives. Second, due to the aerodynamic focusing, the ink is not in direct contact with the nozzle, reducing the proclivity of clogging. Finally, due to the small nature of the droplets (on the order of femtoliters), the approach allows for rapid drying of ink droplets either in flight or on the surface. This has been exploited by numerous recent works to utilize the method to form high-resolution traces [29, 30] and three-dimensional free-standing patterns [31–34].

Aerosol jet printing has been demonstrated for printing QDs for color conversion in a previous report [35]. In this work, the authors specifically print red, green, and blue CdSe QDs on top of UV light-emitting diodes (LEDs). While their results are quite promising, they do not elaborate on the ability to create free-standing structures with significant height to preclude the leakage of the underlying LED. Therefore, for the functional results they incorporate a distributed Bragg reflector (DBR) to filter out the emission from the excitation source. Our work differs from the previous work as we do not use commercially available inks (which may contain additives) and demonstrate sufficiently thick self-standing patterns of QDs which preclude the emission of the underlying LED, ultimately allowing for a simpler fabrication scheme which does not rely on additional color filtering layers.

In this work, we utilize aerosol jet printing to deposit QD CCLs. Aerosol jet printing has numerous advantages, including potential for higher resolution and the ability to print inks with

reduced rheological constraints. However, the most important advantage includes the ability to effectively reduce the solvent volume in-flight allowing for a dryer deposition which can in turn enable the printing of high-aspect ratio features with minimal spreading. To demonstrate these advantages, we print at varied parameters that induce in-flight drying. Specifically, we target two different focus ratios in which the carrier gas volumetric flow rate is modulated to induce the drying of droplets on the periphery of the aerosol stream. We directly demonstrate that when the carrier gas volumetric flow rate is decreased (focus ratio increased), we can dramatically modify the spreading of the printed pattern enabling multi-layer prints which exhibit trace widths of approximately 50 μm with thicknesses of approximately 8 μm. Next, we demonstrate that the effect of trace thickness on both the reduction of blue light leakage and the enhancement of wavelength conversion efficiency. Finally, we utilize the method to directly print patterns onto blue μOLED samples as a technological demonstration of the potential utility of the patterning technique.

## 2 | Results and Discussion

Aerosol jet printing uses two converging gas streams to aerodynamically focus an aerosol on route to substrate impaction. The volumetric flowrate of the two gas streams, the focusing sheath gas and the aerosol laden carrier gas, can be controlled independently. The focus ratio is defined as the sheath gas flow rate divided by the carrier gas flowrate. While the print process relies on minimized mixing between the two streams due to the laminar nature of the flow, by increasing the carrier gas flowrate we can dramatically alter the drying of the droplets at the outer edge of the carrier gas flow column. Droplet drying in flight occurs due to the high vaporization potential of small droplets within a high velocity flow. By increasing the velocity through the introduction of a sheath gas, the effect can be exacerbated at the edge of the aerosol column in which small volume (fl) droplets are accelerated within a dry nitrogen flow. In increasing the drying of the droplets at the edges, we can alter the three-phase contact line and reduce ink spreading as the droplets coalesce on the surface [36].

To demonstrate this, we chose two different focusing ratios in which this effect begins to occur. We show that at a focus ratio (FR) of 3 (sheath gas = 60 SCCM, carrier gas = 20 SCCM), the droplet drying at the edges is minimized, and significant spreading through the equilibrium contact angle settling occurs. Conversely, however, at a focus ratio of 4 (sheath gas = 60 SCCM, carrier gas = 15 SCCM), the three-phase contact line is pinned at the edge of the deposited aerosol leading to minimized spreading outside of the aerosol column width. This can be seen in line profiles of multiple print layers highlighted in Figure 2.

In addition to the proposed mechanism of altering the three-phase contact line, a secondary rheological effect caused by the drying may also play a role in the overall line profile. Specifically, it is plausible that during the drying process, the colloidal inks dry past the gelation point, which would explain the suppression of lateral flow upon deposition [37]. The rapid increase in colloidal concentration at the droplet surface would cause the development of an effective yield stress, which would further inhibit lateral

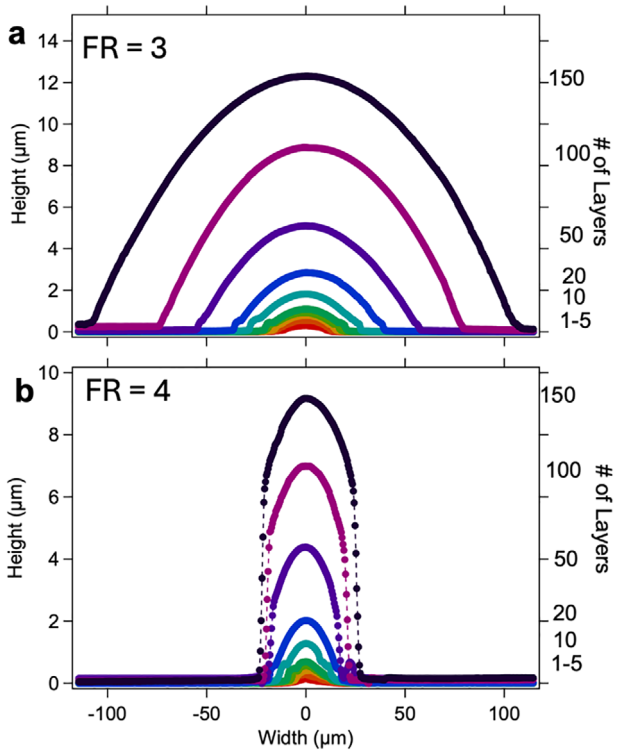


**FIGURE 2** | Cross-sectional height profiles of aerosol jet-printed quantum dot lines printed at varied focus ratios. (A) Printed at a focus ratio of 3 and (B) printed at a focus ratio of 4.

flow. Fully distinguishing between the capillary and rheological contributions would require in situ droplet-impact imaging, which we identify as an important future direction for this work.

Critically, this allows for the printing of multiple layers, up to 150 repeated print passes, in which the overall trace width does not change significantly in higher focus ratio scenariosncreases by a factor of 62, while the width increases by onl. For a focus ratio of 3, while the layer increased in thickness by approximately 40 times, the trace width subsequently increases by a factor of 5. At the higher focus ratio (FR = 4), however, the trace thickness is increased by a factor of 62 while the width is only increased by a factor of 0.41. This effect can also be seen in the optical characteristics of printed lines in Figure 3.

These two focus ratios directly demonstrate the transition point at which the higher sheath gas flowrate begins to influence the deposited pattern. In addition to these specific focus ratios, we completed an experiment with a focus ratio of 6, using all the same conditions and the same carrier gas flow-rate. These results are shown in Figure S1. While we can demonstrate lines with thicknesses as high as 84.83 μm and widths of only 22.50 μm, deleterious edge effects begin to become evident due to the high ratio of gas velocities at the edge of the aerosol column. Of note, the work in this paper is specifically tuned for this specific nozzle diameter (100 μm) and ink chemistry. It is expected that changing these parameters may lead to a varied optimized focus ratio that will require careful experimental or computational optimization.

The impact of directly using the focus ratio to control the morphological characteristics of printed traces is significant,

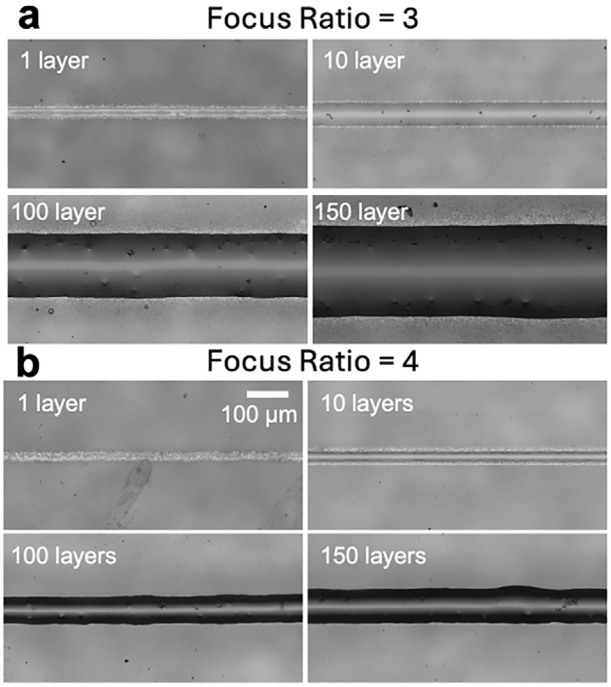


**FIGURE 3** | Optical images of aerosol jet printing quantum dot lines with varied focus ratios. (A) Printed at a focus ratio of 3, and (B) printed at a focus ratio of 4.

as direct control of the trace thickness without significantly compromising trace resolution allows for enhancement of the QD optical characteristics. To demonstrate the effect of thickness on both the conversion efficiency and the blue light leakage reduction caused by the QD layers,- we aerosol jet printed QD films directly on top of prefabricated blue OLEDs. An example optical image, height contour, and height profile from on the squares is shown in the supporting information (Figure S2). The color conversion efficiency is quantified using the following equation:

$$CE = \frac{\int_{570}^{725} emission}{\int_{385}^{550} absorption}$$

where CE is conversion efficiency, the numerator is the visible light emission above 570 nm wavelength, and the denominator is the visible light absorption below 550 nm wavelength. The blue light leakage parameter is defined using the following equation:

$$BLL = \frac{\int_{385}^{550} emission\ (output\ blue\ emission)}{\int_{385}^{550} emission\ (input\ blue\ emission)}$$

where BLL is the blue light leakage, the numerator is the peak intensity of the blue light emitted from the QD-OLED, and the denominator is the peak intensity of the blue light emitted from the blue OLED. This definition allows direct quantification of the fraction of the incident blue light that is not converted by the quantum dots and remains as leaked blue emission.

The results for aerosol jet-printed QD thin films of various thicknesses are presented in Figure 4. Figure 4A shows the luminescence data measured using a half-integrating sphere, with the blue spectrum representing the electroluminescence of the blue OLED reference device. In Figure 4A, the spectra of films at varied thicknesses directly shows the reduction in the blue wavelength and conversion to the red wavelength. As expected, at increased QD film thickness, the blue light peak is significantly reduced. As the thickness is increased, the luminescence within the red color wavelengths remains relatively constant, however, we do directly observe a red shift (magnified within the inset in Figure 4A) in the converted spectra. This is likely due to increased energy loss during the down-conversion process arising from enhanced Förster resonance energy transfer (FRET) and reabsorption among closely packed QDs in the thicker QD films and can also be explained through an enhanced photo quenching due to potentially aggregated quantum dots. Nevertheless, for most of the tested thicknesses, the QD film effectively absorbed the emission from the blue OLED, resulting in strong red emission after color conversion.

To further confirm that this red shift originates from thickness-dependent packing effects rather than from QD degradation during the aerosol jet printing process, we compared the normalized photoluminescence spectra of the thinnest (3.46 µm) aerosol-jet-printed and spin-coated QD films in the red emission region (Figure S3). The peak position, spectral shape, and linewidth are nearly identical between the two films, and no additional long-wavelength emission associated with trap or defect states is observed in the AJP film. This indicates that the intrinsic emissive properties of the QDs are well preserved, and that the AJP process does not induce significant surface ligand detachment or defect-related degradation.

Through a quantification of the CE (Figure 4B) the reduction in CE becomes clear, with the CE reaching near stagnation at 16% as the film thickness approaches 19 µm. The BLL (Figure 4C) as expected, follows the opposite trend in which it is thoroughly quenched as the film thickness reaches above 7 µm. With no additional light filtering, we are able to directly demonstrate that the BLL falls below 0.25% at film thicknesses above 7 µm. This behavior is enabled by the aerosol jet printing of polymer-free QD inks. Additionally, the high velocity impaction induced by the process allows for the QDs to be more densely populated within the film enhancing the blue light leakage reduction. Of note, however, is that the claim regarding the packing density of the QD layer is based on indirect, optical evidence. Future work will look to quantify the packing density directly through high resolution TEM imaging. Based on the results demonstrated, an optimal thickness of approximately 7.5 µm is identified in which the QD CE and BLL values are 17.6% and 0.24%, respectively.

Figure 4D presents the actual emission images of samples x and y to verify that only the QD light is visible without blue leakage. A substrate contains four emitting pixels, with the top two pixels being QD-OLEDs with printed QD film, and the bottom two pixels serving as reference blue OLEDs. In the QD-OLED, the left side represents sample x and the right side represents sample y. Upon visual inspection, it was confirmed that the QD-OLED pixels emitted pure red light from the QDs, rather than a purple color mixed with blue light.

In Figure 5 we present the data for three different thicknesses, 4.16, 7.56, and 19.28 µm. All thicknesses may be considered

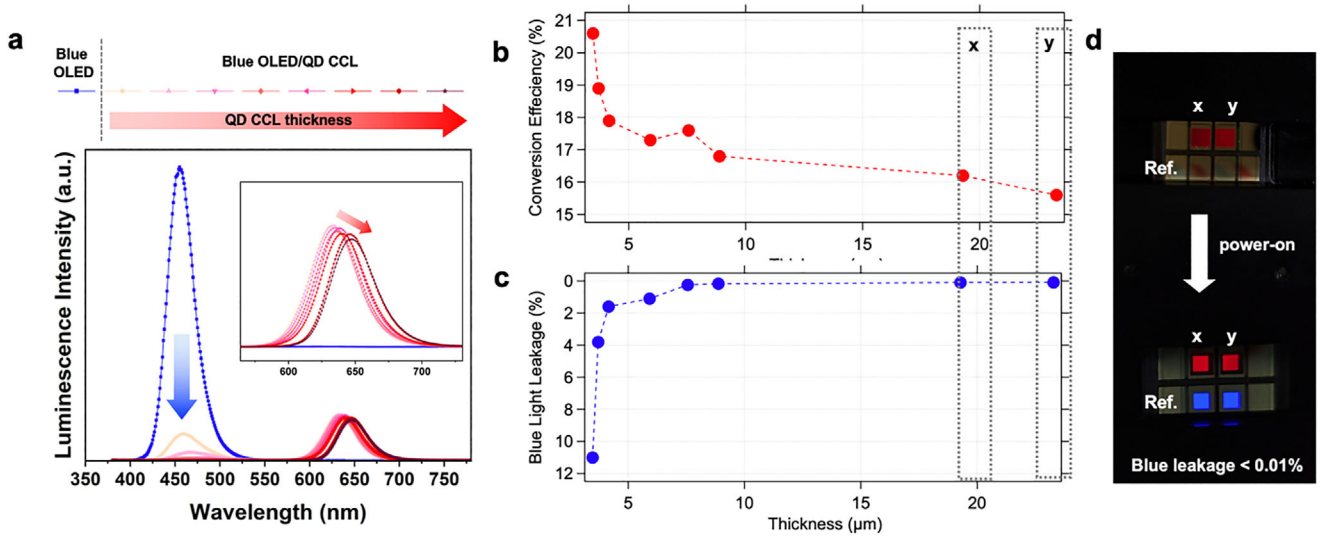


**FIGURE 4** | Optical characteristics of aerosol jet-printed quantum dot thin films at varied thickness. (A) Spectra modification presented as luminescence characteristics at specific optical wavelengths. (B) Quantification of color conversion efficiency and (C) blue light leakage as a function of film thickness. (D) photograph of specific films printed directly adjacent to reference blue OLEDs in both the off- and on-state.

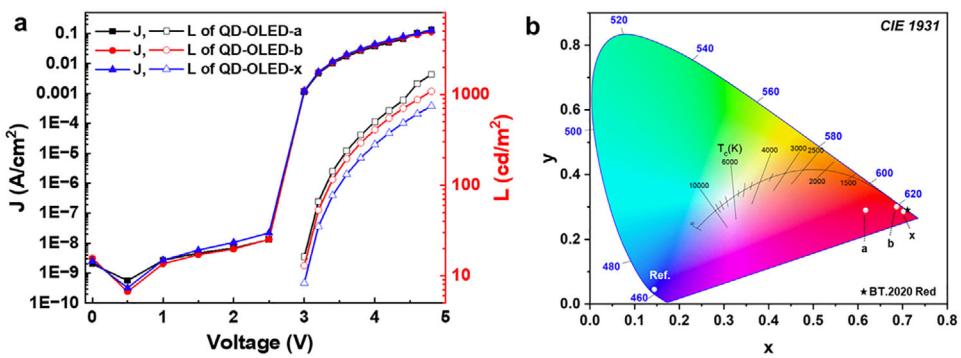


**FIGURE 5** | Optical characteristics for three specific aerosol jet printed QD film thickness, 4.16 (a) and 7.56 (b), and 19.28 μm(x). (A) Current density–voltage (*J–V*) (left axis) and luminance–voltage (*L–V*) characteristics (right axis) of QD-OLEDs (a, b, and x) showing the variation in electrical performance and brightness as a function of applied voltage. (B) CIE 1931 chromaticity diagram showing the color coordinates of the OLED as a Ref. and QD-OLEDs, with the BT.2020 red primary (x = 0.708, y =0.292) indicated for comparison. QD-OLED-a, QD-OLED-b, and QD-OLED-x exhibit color coordinates approaching the desired red region, with slight variation in the chromaticity values between the samples.

optimal, depending on the specific application. The sample with a QD film thickness of 4.16 μm is designated as QD-OLED-a, the one with a thickness of 7.56 μm as QD-OLED-b, and the one with a thickness of 19.28 μm as QD-OLED-x. Figure 5A shows the *J–V–L* data, confirming that all samples exhibit similar electrical characteristics regardless of the QD film thickness. No statistically significant change is observed in the electrical performance of QD-OLEDs, which means that the thin-film encapsulation stably protected the OLED during the aerosol-jet printing process. The luminance versus voltage curve exhibits a monotonic decrease in luminance as the thickness of the QD film increases from a to b to x. This trend is consistent with the results in Figure 4, indicating that while the blue light significantly decreases with increasing QD film thickness, the corresponding increase in QD light is not sufficient to maintain the overall luminance of the device. Figure 5B presents the chromaticity coordinates of the QD-OLEDs in the CIE 1931 color space. Upon introducing QD CCLs to the blue OLED, the chromaticity shifts from the blue region toward the red region. This shift is attributed to the increased ratio of red to blue emission, resulting from efficient color conversion and strong absorption of blue light by the QD layer. As the thickness of the QD film increases, the chromaticity coordinates progressively move deeper into the red region and, when compared with the BT.2020 red primary, become increasingly similar to the BT.2020 red coordinate. Notably, at the thickest QD film (x), the chromaticity reaches (x, y) = (0.702, 0.286), which is very close to the BT.2020 red primary (x = 0.708, y = 0.292).

Printing relatively thin, additive-free QD films offers a particularly attractive option for integrating QD CLLs within OLEDoS. In this study, the aerosol-jet printing technique we developed allows precise control over the printed line width, making it adaptable to displays with various pixel sizes. In Figures 4 and 5, we examined the application of a QD film onto a lab-scale blue OLED unit device using aerosol-jet printing.

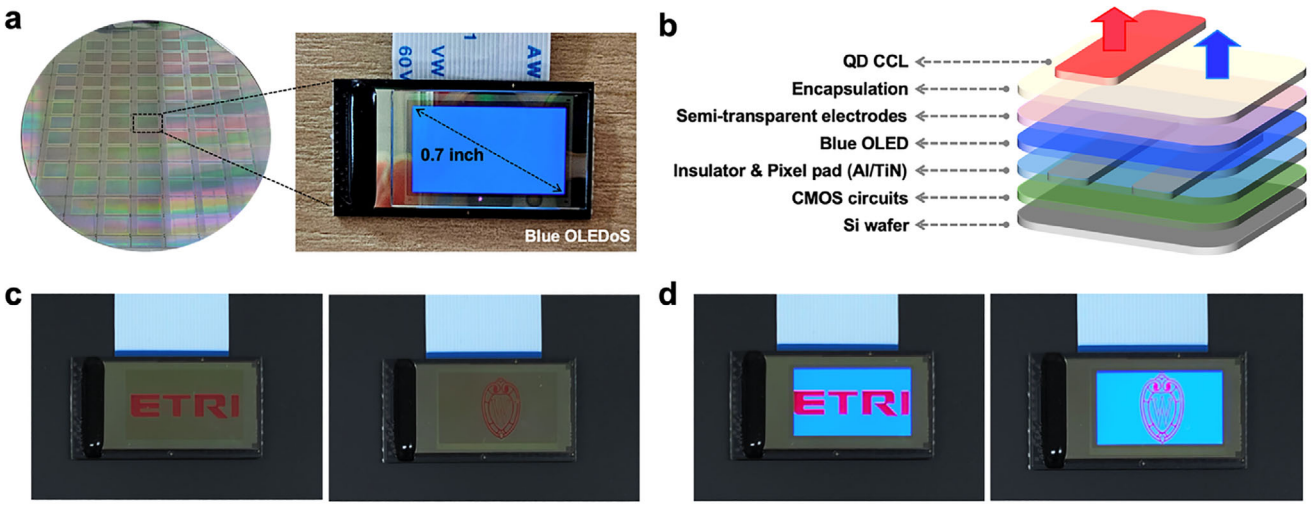


**FIGURE 6** | Direct printing of quantum-dot color-conversion layers on OLED microdisplays. (A) Blue OLED-on-silicon (OLEDoS) microdisplay used in this study, including a photograph of the 0.7-inch active area and the corresponding die layout. (B) Schematic of the top-emitting blue OLEDoS device stack fabricated on a CMOS backplane, consisting of CMOS circuits on a Si wafer, Al/TiN pixel electrodes, blue OLED layers, semi-transparent top electrodes, encapsulation, and the printed quantum-dot color-conversion layer (QD CCL). (C) Dark-state images of the OLEDoS after aerosol-jet printing of red QD patterns, showing printed institutional logos (ETRI and University of Wisconsin–Madison) with no device illumination. (D) Fully lit operation of the QD-patterned OLEDoS, demonstrating efficient blue-to-red color conversion with high color purity and no observable blue leakage, even in the absence of a color filter.

In Figure 6, we extended this approach to a 0.7-inch OLED microdisplay, specifically an OLEDoS. Figure 6A shows an image of the fabricated blue OLEDoS, which was produced using an 8-inch wafer process. The OLEDoS has an aspect ratio of 16:9 and a pixel density of 3,147 ppi. The blue OLEDoS used in this study features the structure shown in Figure 6B. It was fabricated using a CMOS substrate and designed as a top-emitting OLED which has the same structure as the lab-scale blue OLED unit except that the lower electrode is changed from ITO/Ag/ITO to Al/TiN. A QD CCL was formed on the blue OLEDoS via aerosol-jet printing. In Figure 6C,D, we displayed the logos of ETRI and the University of Wisconsin-Madison. Figure 6D shows an image of the display in operation. As shown, after the QD printing process, a vibrant red color is achieved without any blue leakage, even in the absence of a color filter. This demonstrates the effectiveness of the QD CCL in achieving pure red emission.

## 3 | Conclusion

Printable QD color conversion films have the potential to enable high-throughput, additive modification of single-color monolithically integrated μLED and μOLED displays. In this work, we directly demonstrate the advantages that aerosol jet printing presents toward the spatially resolved deposition of QD films. First, the ability to induce droplet drying at the outer radial circumference can effectively pin the three-phase contact angle of the printed pattern. We have demonstrated that this drastically reduces liquid spreading and can enable high-resolution printed films at substantial thicknesses approaching 10 μm without compromising in trace resolution. The other specific advantage demonstrated is the technique's ability to process reduced-viscosity QD inks that contain no polymeric additives. The printing of pure QD inks with a high velocity of substrate impingement enables thin films (< 7 μm) that exhibit unprecedented BLL metrics while maintaining sufficiently high CE metrics. Lastly, we directly demonstrate the ability to print high-resolution printed QD patterns onto prefabricated μOLED displays. Such a technique can enable RGB-capable μOLED displays with reduced manufacturing complexity.

## 4 | Experimental Section

### 4.1 | Ink Preparation

QD inks were prepared by mixing 955 μL of toluene (Sigma–Aldrich), 10 μL of terpineol (10% v/v, Frontier Scientific), and 35 μL of CdSe/CdZnS (core–shell) QD stock solution (oleic acid-capped CdSe/CdZnS quantum dots (Nano dot-HE-series) (Powerlogics, Korea)).

### 4.2 | Aerosol Jet Printing and Profile Characterization

For printing high-resolution lines, the inks were aerosolized using an ultrasonic transducer current of 0.20–0.25 A. The sonication bath temperature was maintained at 20°C. A 100 μm nozzle was used. The sheath gas flow rate was maintained at a constant volumetric flow rate of 60 SCCM. The carrier gas flow rate was varied from 15 SCCM (focus ratio = 4) and 20 SCCM (focus ratio = 3). The standoff distance between the nozzle and the substrate was 2.4 mm, and the platen temperature was maintained at 37°C. The linear print speed was 2 mm/s.

For the direct deposition of the QD ink onto the OLED substrate, a larger nozzle of 200 μm was used to facilitate faster printing. The sonication bath temperature was maintained at 20°C. The sheath and carrier gas flow rates were 92 and 23 SCCM, respectively,

resulting in a focus ratio of 4. The larger nozzle and carrier gas flow rate allowed for an increased printing speed of 5 mm/s and the platen was held at room temperature. The standoff distance was also maintained from the line printing experiments at 2.4 mm.

The film thickness and height profiles of the lines were characterized using an optical profilometer (New View 9000, Zygo), while the heights of the QD layers directly on top of the μOLED samples were characterized using an Olympus LEXT OLS5100 3D Laser Scanning Microscope.

## 4.3 | Optical Characterization

The electrical and optical characteristics of OLED and OLEDs with QD CCL were measured by a using a source meter (Keithley 238), a spectrometer (CS2000, Konica Minolta) and a total luminous flux measurement system (HM series, Otsuka Electronics) with a half-integrating sphere.

## 4.4 | μOLED Display Fabrication

A silicon CMOS backplane served as the substrate for the OLED-on-silicon (OLEDoS) fabrication. The backplane was prepatterned with integrated pixel circuits and thoroughly cleaned to eliminate organic residues and surface impurities. OLED layers were deposited onto the CMOS backplane through thermal evaporation, following a process similar to the previously described OLED fabrication technique. For encapsulation and long-term protection of the OLEDoS, a multilayer thin film encapsulation (TFE) was employed, consisting of $Al_2O_3/SiN_x$/transparent polymer layer. Compared to standard OLED unit devices, in OLEDoS, an additional transparent polymer layer was applied on top of the $SiN_x$ layer to protect against damage during the sawing process on an 8-inch wafer and to accommodate the via etching process of the TFE, which is necessary for the wire bonding process to drive the OLEDoS. A QD film was applied directly onto the OLEDoS surface using aerosol jet printing. Future work should include a focus on improving the conversion efficiency, while also improving the overall print resolution through advanced, aerosol focusing techniques.


### Acknowledgements

The authors acknowledge funding support provided through the College of Engineering at UW-Madison and through the Vice Chancellor for Research and Graduate Education. This work was partly supported by D2P's Draper TIF program as well as in part by Electronics and Telecommunications Research Institute (ETRI) grant funded by the Korean Government [26ZC1200, Research on Ultra-Realistic Spatial Device Technology] and in part by Institute of Information & Communications Technology Planning & Evaluation (IITP) grant funded by the Korean Government (MSIT) (No 2022-0-00026, Near-eye light field device technology development for hyper-realistic metaverse service).


### Conflicts of Interest

The authors declare no conflicts of interest.

### Data Availability Statement

The data that support the findings of this study are available from the corresponding author upon reasonable request.

### References


1. J. Chen, Q. Zhao, B. Yu, and U. Lemmer, "A Review on Quantum Dot-Based Color Conversion Layers for Mini/Micro-LED Displays: Packaging, Light Management, and Pixelation," *Advanced Optical Materials* 12 (2024): 2300873.

2. R. Tangirala, E. Lee, C. Hotz, et al., "86-2: Color Conversion Using Quantum Dots for LCD, OLED, and MicroLED Displays," in *Digest of Technical Papers - SID International Symposium*, 51 (Blackwell Publishing Ltd, 2020): 1299–1302, https://doi.org/10.1002/sdtp.14120.

3. Z. Hu, Y. Yin, M. U. Ali, et al., "Inkjet Printed Uniform Quantum Dots as Color Conversion Layers for Full-Color OLED Displays," *Nanoscale* 12, no. 3 (2020): 2103–2110, https://doi.org/10.1039/c9nr09086j.

4. T. Erdem and H. V. Demir, "Color Science of Nanocrystal Quantum Dots for Lighting and Displays," *Nanophotonics* 2 (2013): 57–81, https://doi.org/10.1515/nanoph-2012-0031.

5. F. Qin, C. Liu, W. Wu, et al., "Inkjet Printed Quantum Dots Color Conversion Layers for Full-Color Micro-LED Displays," *Electronic Materials Letters* 19, no. 1 (2023): 19–28, https://doi.org/10.1007/s13391-022-00373-5.

6. G. Li, M. C. Tseng, Y. Chen, et al., "Color-Conversion Displays: Current Status and Future Outlook," *Light: Science and Applications* 13 (2024): 301, https://doi.org/10.1038/s41377-024-01618-8.

7. B. Xie, R. Hu, and X. Luo, "Quantum Dots-Converted Light-Emitting Diodes Packaging for Lighting and Display: Status and Perspectives," *Journal of Electronic Packaging* 138 no. 2 (2016): 020803, https://doi.org/10.1115/1.4033143.

8. S. Y. Park, S. Lee, J. Yang, and M. S. Kang, "Patterning Quantum Dots via Photolithography: A Review," *Advanced Materials* 35 (2023): 2300546, https://doi.org/10.1002/adma.202300546.

9. B. L. Huang, T. L. Guo, S. Xu, Y. Ye, E. G. Chen, and Z. X. Lin, "Color Converting Film With Quantum-Dots for the Liquid Crystal Displays Based on Inkjet Printing," *IEEE Photonics Journal* 11, no. 3 (2019): 1–9, https://doi.org/10.1109/JPHOT.2019.2911308.

10. D. Y. Kim, Y. J. Han, J. Choi, C. Sakong, B. K. Ju, and K. H. Cho, "Inkjet Printed Quantum Dot Film Formed by Controlling Surface Wettability for Blue-to-Green Color Conversion," *Organic Electronics* 84 (2020): 105814, https://doi.org/10.1016/j.orgel.2020.105814.

11. Y. Wang, J. A. Pan, H. Wu, and D. V. Talapin, "Direct Wavelength-Selective Optical and Electron-Beam Lithography of Functional Inorganic Nanomaterials," *ACS Nano* 13, no. 12 (2019): 13917–13931, https://doi.org/10.1021/acsnano.9b05491.

12. D. B. Dement, M. K. Quan, and V. E. Ferry, "Nanoscale Patterning of Colloidal Nanocrystal Films for Nanophotonic Applications Using Direct Write Electron Beam Lithography," *ACS Applied Materials & Interfaces* 11, no. 16 (2019): 14970–14979, https://doi.org/10.1021/acsami.9b01159.

13. Z. Gao, J. Shi, and G. Yang, "Quantum Dots Photoresist for Direct Photolithography Patterning," *Advanced Optical Materials* 12 (2024): 2401106, https://doi.org/10.1002/adom.202401106.

14. H. Yoshida, S. Nakatani, Y. Usui, D. Wakabayashi, and F. Ohtsuka, "High-Precision and High-Stability Inkjet Printing Technology for QD Color Converter-Type Micro-LED Display," *Journal of the Society for Information Display* 31, no. 5 (2023): 316–327, https://doi.org/10.1002/jsid.1218.

15. L. Wang, S. Shi, L. Yin, et al., "Water-Soluble Quantum Dots for Inkjet Printing Color Conversion Films with Simultaneous High Efficiency and Stability," *ACS Applied Materials & Interfaces* 16, no. 4 (2024): 5050–5057, https://doi.org/10.1021/acsami.3c13244.

16. FujiFilm. Dimatix Materials Cartridge – Samba Cartridge. Santa Clara, 2021.

17. Y. Lin, W. Huang, M. Zhanghu, and Z. Liu, "Ultra-Thick Inkjet-Printed Quantum Dots Layer for Full-Color Micro-LED Displays," *Optics Express* 31, no. 20 (2023): 31818, https://doi.org/10.1364/oe.498974.

18. K. Yan, J. Li, L. Pan, and Y. Shi, "Inkjet Printing for Flexible and Wearable Electronics," *APL Materials* 8, no. 12 (2020): 120705, https://doi.org/10.1063/5.0031669.

19. Y. Wang, Y. Luo, X. Kong, et al., "Patterning Technologies of Quantum Dots for Color-Conversion Micro-LED Display Applications," *Nanoscale* 17 (2024): 1764–1789, https://doi.org/10.1039/d4nr03925d.

20. B. Huang, E. Chen, L. Sun, and T. Guo, "Quantum-Dot Color Conversion Film Patterned by Screen Printing and Overprinting Process for Display Backlights," *Opt Laser Technol* 145 (2022): 107486, https://doi.org/10.1016/j.optlastec.2021.107486.

21. A. Tang, Y. Liu, Q. Wang, et al., "A New Photoelectric Ink Based on Nanocellulose/CdS Quantum Dots for Screen-Printing," *Carbohydrate Polymers* 148 (2016): 29–35, https://doi.org/10.1016/j.carbpol.2016.04.034.

22. B. H. Kim, M. S. Onses, J. B. Lim, et al., "High-Resolution Patterns of Quantum Dots Formed by Electrohydrodynamic Jet Printing for Light-Emitting Diodes," *Nano Letters* 15, no. 2 (2015): 969–973, https://doi.org/10.1021/nl503779e.

23. X. Wang, Z. Chen, H. Zhou, et al., "Printing Quantum Dot Color Conversion Layer in Etch Pits Using EHD Technology Based on Mini-LED," *Applied Physics Letters* 126, no. 1 (2025): 011106, https://doi.org/10.1063/5.0244782.

24. H. Wang, Y. Zhang, Y. Liu, et al., "High-Efficiency and High-Resolution Patterned Quantum Dot Light Emitting Diodes by Electrohydrodynamic Printing," *Nanoscale Advances* 5, no. 4 (2023): 1183–1189, https://doi.org/10.1039/d2na00862a.

25. S. Kim, S. Kang, S. Baek, et al., "Highly Thin Film with Aerosol-Deposited Perovskite Quantum Dot/Metal Oxide Composite for Perfect Color Conversion and Luminance Enhancement," *Chemical Engineering Journal* 441 (2022): 135991, https://doi.org/10.1016/j.cej.2022.135991.

26. S. Zou, Y. Li, and Z. Gong, "Wafer-Scale Patterning of High-Resolution Quantum Dot Films with a Thickness over 10 Mm for Improved Color Conversion," *Nanoscale* 15, no. 45 (2023): 18317–18327, https://doi.org/10.1039/d3nr04615j.

27. E. B. Secor, "Principles of Aerosol Jet Printing," *Flexible and Printed Electronics* 3 (2018): 035002, https://doi.org/10.1088/2058-8585/aace28.

28. J. Q. Feng, A. Ramm, and M. J. Renn, "A Quantitative Analysis of Overspray in Aerosol Jet® Printing," *Flexible and Printed Electronics* 6 (2021): 045006, https://doi.org/10.1088/2058-8585/ac3019.

29. T. Ma, Y. Li, H. Cheng, et al., "Enhanced Aerosol-Jet Printing Using Annular Acoustic Field for High Resolution and Minimal Overspray," *Nature Communications* 15, no. 1 (2024): 6317, https://doi.org/10.1038/s41467-024-50789-w.

30. B. I. Guyll, L. D. Petersen, C. L. Pint, and E. B. Secor, "Enhanced Resolution, Throughput, and Stability of Aerosol Jet Printing via In Line Heating," *Advanced Functional Materials* 34, no. 28 (2024): 2316426, https://doi.org/10.1002/adfm.202316426.

31. J. Q. Feng and M. J. Renn, "Aerosol Jet® Direct-Write for Microscale Additive Manufacturing," *Journal of Micro and Nano Science and Engineering* 7, no. 1 (2019): 011004, https://doi.org/10.1115/1.4043595.

32. S. Jahan, C. Hu, B. Yuan, S. M. Ritchie, and R. Panat, "Aerosol Jet 3D Printing of Gold Micropillars and Their Behavior under Compressive Loads," *Additive Manufacturing* 92 (2024): 104385, https://doi.org/10.1016/j.addma.2024.104385.

33. B. N. Smith, P. Ballentine, J. L. Doherty, et al., "Aerosol Jet Printing Conductive 3D Microstructures from Graphene Without Post-Processing," *Small* 20, no. 12 (2024): 2305170, https://doi.org/10.1002/smll.202305170.

34. M. Seiti, O. Degryse, and E. Ferraris, "Aerosol Jet® Printing 3D Capabilities for Metal and Polymeric Inks," *Materials Today: Proceedings, Elsevier Ltd* 70 (2022): 38–44, https://doi.org/10.1016/j.matpr.2022.08.488.

35. H.-V. Han, H.-Y. Lin, C.-C. Lin, et al., "Resonant-Enhanced Full-Color Emission of Quantum-Dot-Based Micro LED Display Technology," *Optics Express* 23, no. 25 (2015): 32504, https://doi.org/10.1364/oe.23.032504.

36. B. I. Guyll, B. L. Sanford, C. L. Pint, and E. B. Secor, "Controlling Droplet Evaporation in Aerosol Jet Printing to Understand and Mitigate Overspray," *Small Science* 5 (2025): 2500069, https://doi.org/10.1002/smsc.202500069.

37. L. Gamba, S. Diaz-Arauzo, M. C. Hersam, and E. B. Secor, "Aerosol Jet Printing of Phase-Inversion Graphene Inks for High-Aspect-Ratio Printed Electronics and Sensors," *ACS Applied Nano Materials* 6, no. 22 (2023): 21133–21140, https://doi.org/10.1021/acsanm.3c04207.

## Supporting Information

Additional supporting information can be found online in the Supporting Information section.

**Supporting File**: adom71344-sup-0001-SuppMat.docx.